ARTICLES

Effect of inertia on drop breakup under shear

Yuriko Y. Renardy[a)]
Department of Mathematics and ICAM, 460 McBryde Hall, Virginia Tech, Blacksburg, Virginia 24061-0123

Vittorio Cristini[b)]
Department of Chemical Engineering and Materials Science, 151 Amundson Hall, 421 Washington Avenue S.E., University of Minnesota, Minneapolis, Minnesota 55455-0132

(Received 23 May 2000; accepted 6 October 2000)

A spherical drop, placed in a second liquid of the same density and viscosity, is subjected to shear between parallel walls. The subsequent flow is investigated numerically with a volume-of-fluid continuous-surface-force algorithm. Inertially driven breakup is examined. The critical Reynolds numbers are examined for capillary numbers in the range where the drop does not break up in Stokes flow. It is found that the effect of inertia is to rotate the drop toward the vertical direction, with a mechanism analogous to aerodynamic lift, and the drop then experiences higher shear, which pulls the drop apart horizontally. The balance of inertial stress with capillary stress shows that the critical Reynolds number scales inversely proportional to the capillary number, and this is confirmed with full numerical simulations. Drops exhibit self-similar damped oscillations towards equilibrium analogous to a one-dimensional mass-spring system. The stationary drop configurations near critical conditions approach an inviscid limit, independent of the microphysical flow- and fluid-parameters.
 [DOI: 10.1063/1.1331321]

I. INTRODUCTION

The goal of this article is to examine the effect of inertia on the idealized problem of an isolated drop subjected to simple shear in a matrix liquid. The undeformed radius is a, the plate separation is d, and the computational box has periodic boundary conditions in the horizontal directions. The undisturbed velocity field is $\mathbf{u}=\dot{\gamma}z\mathbf{i}$, where $\dot{\gamma}$ is the imposed shear rate. There are seven dimensionless parameters: the viscosity ratio of the drop to matrix liquids $\lambda=\mu_d/\mu_m$, the capillary number $\mathrm{Ca}=\mu_m\dot{\gamma}a/\sigma$, the Reynolds number $\mathrm{Re}=\rho_m\dot{\gamma}a^2/\mu_m$, the dimensionless plate separation d/a, and dimensionless spatial periodicities in the x and y directions. In order to examine trends, we focus on the case $\lambda=1$, which is the viscosity ratio that has received the most attention in the literature.[1–6]

It is known that for Stokes flow, capillary numbers in the range 0 to 0.43 yield steady states with egg-shaped drops. On the other hand, the addition of sufficient inertia induces breakup for these capillary numbers. In Ref. 7, Sec. V is concerned with inertially driven breakup (cf. their Figs. 17–20). The critical Reynolds number is small for Ca close to 0.4, but increases rapidly as Ca decreases. At each capillary number, the increase in Reynolds number deforms the drop from ellipsoidal to elongated. In comparison with the velocity fields for Stokes flow, the increase in Re leads to a markedly stronger velocity field in the drop region. For example, steady solutions show strong vortical motions inside the drop just below the critical Reynolds number. This is accompanied by an increase in the Taylor deformation parameter D for the steady-state solutions, as the Reynolds number is increased. There are three trends for the overall effect of inertia. First, inertia rotates the drop, so that at higher Reynolds numbers, the steady states are more aligned toward the vertical than in Stokes flow and therefore the drop experiences greater shear. Second, in Stokes flow, the flow inside the drop consists of a single vortical swirl, whereas inertia induces a second vortical swirl evident in the plots for Reynolds numbers 10 and 20. The two vortices sit at the top and bottom ends of the drop. Third, the length of the drop in steady states just below breakup shortens as inertia increases, and the symmetry across the mid-plane of the steady state, evident in Stokes flow, is lost. These trends raise two open questions: what is the mechanism for breakup under inertia, and what is the large Reynolds number asymptotics for the critical curve? These issues are addressed in this article.

II. LARGE REYNOLDS NUMBER BEHAVIOR

In Stokes flow, the primary parameter is the capillary number, which is a measure of the viscous force causing deformation relative to interfacial tension force which keeps the drop together. An order of magnitude estimate of breakup conditions is derived with a balance of the viscous stress and capillary stress, $\mu\dot{\gamma}\sim\sigma/a$, which yields $\mathrm{Ca}\sim 1$.

[a)]Electronic mail: renardyy@math.vt.edu
[b)]Electronic mail: cristini@cems.umn.edu

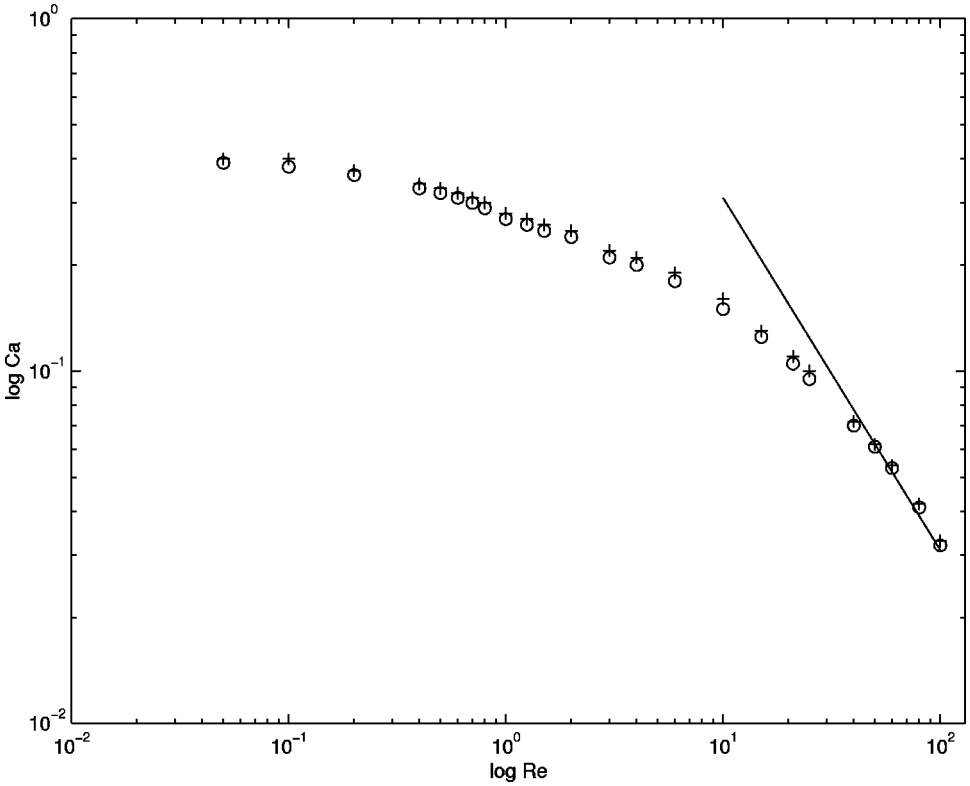

FIG. 1. Log-log plot of Re vs Ca, $\lambda = 1$, equal densities. + drop breakup, ○ steady state solution, — line. Re.Ca =constant.

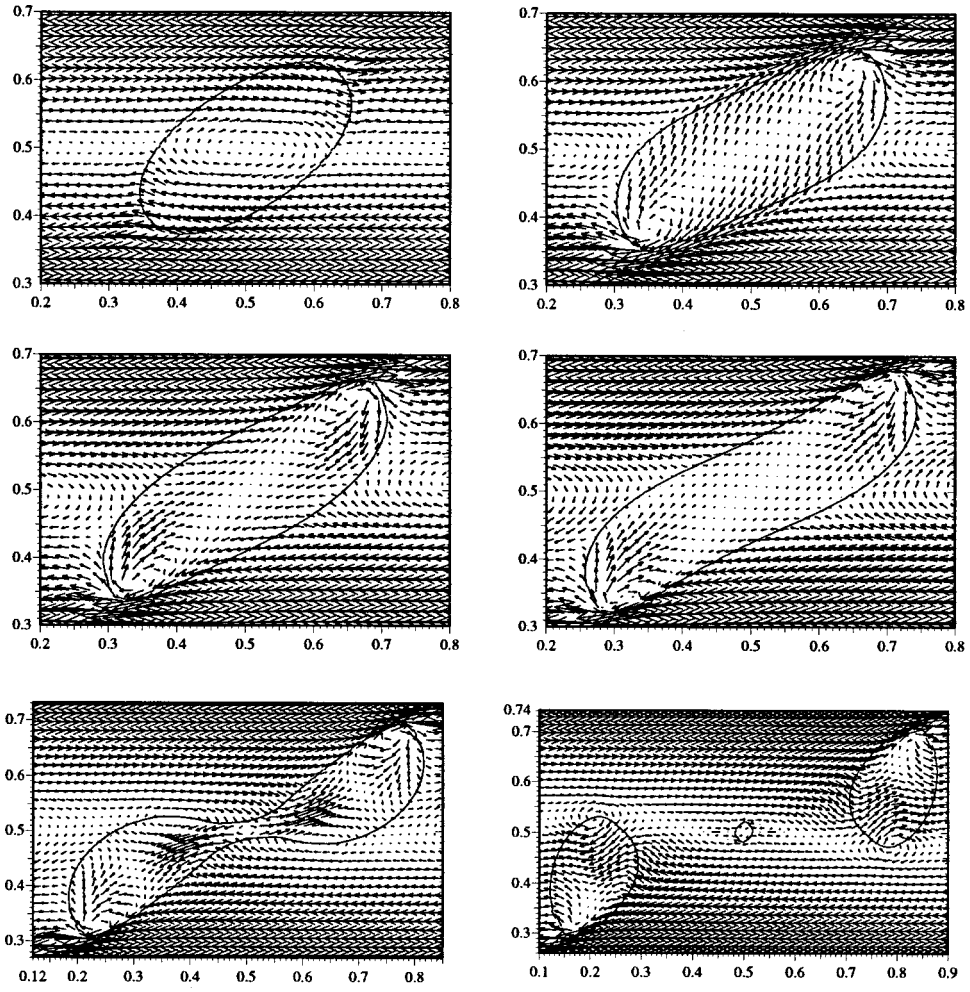

FIG. 2. Velocity vector plots for the cross-section through the center of the drop in the *x*-*z* plane. Left to right, top to bottom: $t=0.9$, 2.4, 4, 7.5, 20, 22.5 s. Re=60, Ca=0.054.

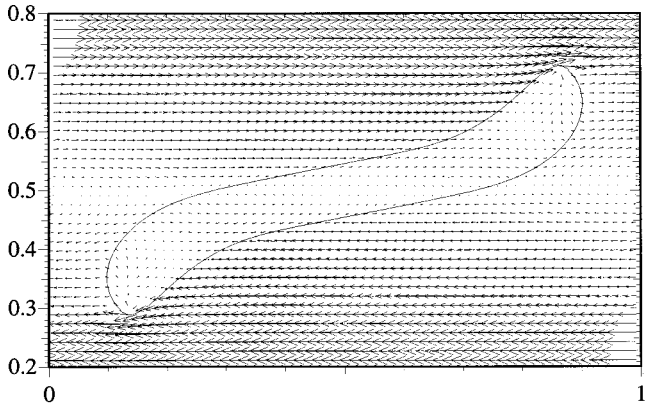

FIG. 3. Velocity vector plot for the cross-section through the center of the drop in the *x*-*z* plane, just before breakup. Re=100, Ca=0.042. 128×64 ×128 mesh, 1×0.5×1 domain. $a=0.125$. The drop elongates and rotates to a high angle.

For large Reynolds numbers, the Reynolds stress is of order $\rho|\mathbf{v}|^2 \sim \rho\dot{\gamma}^2 a^2$. This is balanced by capillary stresses of order σ/a. The critical condition is, upon division by the viscous stress $\mu\dot{\gamma}$,

$$\mathrm{Re} \sim 1/\mathrm{Ca}. \tag{2.1}$$

This is illustrated in the numerical results of Fig. 1. At the points represented on this figure, a full simulation of the initial value problem, together with the Navier–Stokes equations and the continuous surface force formulation[8–11] with our code SURFER++ was conducted. The log–log plot of critical conditions shows that for larger Reynolds numbers, the critical conditions follow the line of slope -1.

The computations were performed on the domain 1 ×0.5×1, with a 64×32×64 mesh, and initial drop radius $a=0.125$, timesteps $10^{-3}\dot{\gamma}^{-1}$, unless otherwise indicated. All results in this article concern viscosity ratio $\lambda=1$ and equal densities.

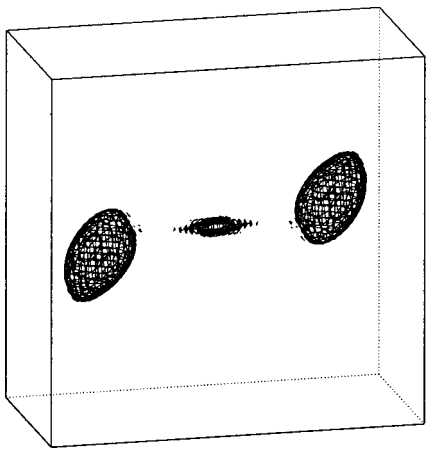

FIG. 4. Three-dimensional picture just after breakup at Re=50, Ca=0.07.

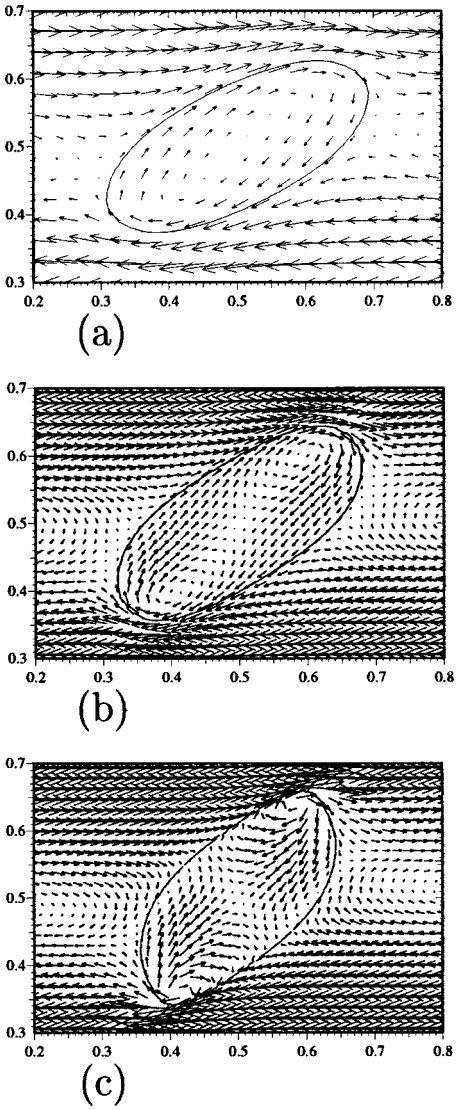

FIG. 5. Velocity vector plot for the cross-section through the center of the drop in the *x*-*z* plane, just below criticality. (a) Re=1, Ca=0.27, $L/a=1.8$, $\theta=25$ deg. (b) Re=10, Ca=0.15, $L/a=1.9$, $\theta=23°$. (c) Re=60, Ca =0.053, $L/a=1.52$, $\theta=53°$.

III. MECHANISM FOR INERTIALLY DRIVEN BREAKUP

A. Lift and counter-lift

Figure 2 shows a typical sequence of events to inertially driven breakup. These velocity vector plots show that as the drop is pulled apart by the base flow, vortical swirls develop at the two ends, with little going on in the neck region. The difference with Stokes flow is the upward tilt, induced by an effect analogous to flying in inviscid flow. When inertia is important, we may invoke Bernoulli's equation, which states that pressure $p+\rho|\mathbf{v}|^2/2$ is a constant along each streamline. In the matrix liquid, therefore, the large velocities near the tips induce negative pressures there relative to the pressure elsewhere. The resulting suction leads to further tilting of the drop. This is an aerodynamic lift on one end, together with a counter-lift at the other end. The drop is then exposed to ever larger shear with further tilting, which allows the base shear flow to pull away the ends. This scenario is similar for higher

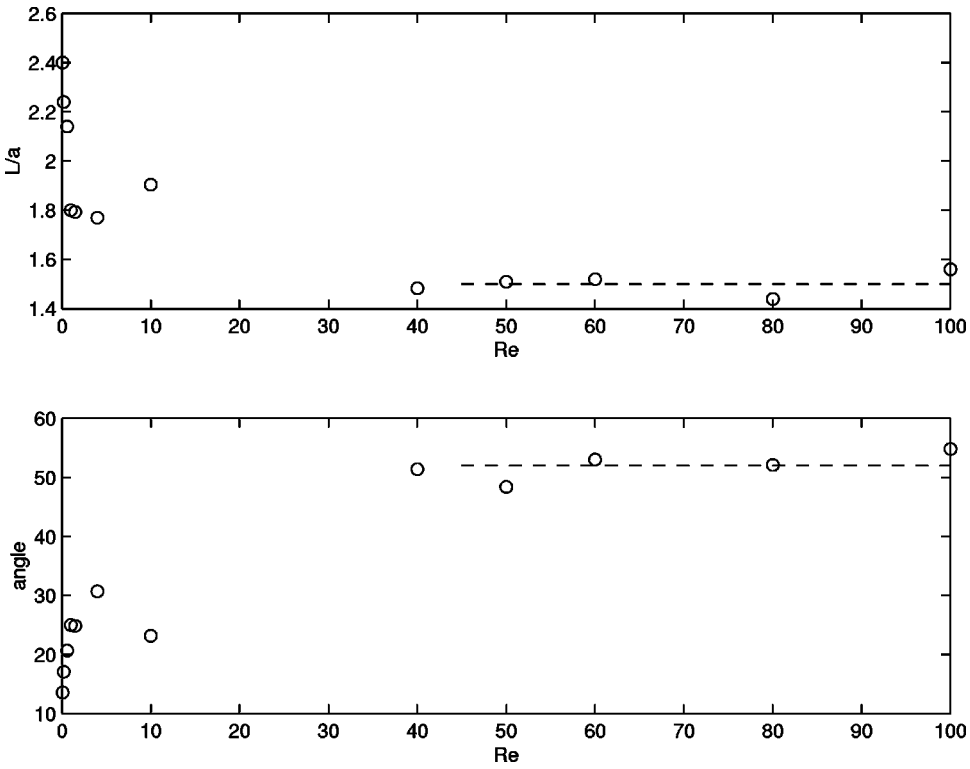

FIG. 6. The half-length L/a and angle of tilt θ vs Re for near-critical solutions. The dashed line is a fit to the constant data at high Re.

Reynolds numbers. The bending up of the end of the drop is reminiscent of the formation of 2D fingers when surface tension is added in simulations of inviscid Kelvin–Helmholtz instability.[12]

With increase in the capillary number, the stretching induced by viscous shear becomes stronger. As in Stokes flow, this leads to longer necks before breakup. A higher Re case is shown in Fig. 3 at Re=100, Ca=0.042 in. The difference with Stokes flow is again the high angle of tilt. Figure 4 is a three-dimensional plot after breakup for Re=50, Ca=0.07.

B. Inertia-induced wobbling

Figure 5 shows the cross-sectional velocity fields for long-time solutions just below criticalities. Plot (a) is a steady state solution (vectors are plotted at fewer grid points; the grid size is the same for all plots). Plot (c) undergoes slight oscillations in the length-wise direction as it approaches steady state. The diagnostics are the half-length L, half-breadth B, and angle θ with the x-axis. Inertia increases from (a) to (c), and tilts the drop. At low Reynolds numbers, there is a single vortex in the interior. As the Reynolds number increases, the vortical motion inside the drop begins to separate into two vortices. This is evident by Re=10. The angle of tilting increases, the drop is subjected to stronger shear and the two vortical swirls inside the drop become more evident. At Re=60, there are four vortical swirls. At higher Reynolds numbers, the competition between the lift exerted on the drop versus pulling by the shear leads to shortening for long-time solutions.

Figure 6 shows results for near-critical capillary numbers. The plots demonstrate that for large Reynolds numbers, the length and angle of inclination approach constants. The scatter of the data is explained by the variation in the deviation from critical capillary numbers. The large Reynolds number result is approximately an inviscid limit, in which the time-dependent momentum equation is a balance

$$\mathbf{u}_t + (\mathbf{u}\cdot\nabla\mathbf{u}) \sim -\nabla\left(\frac{p}{\rho}\right), \tag{3.1}$$

and the stress balance across the fluid interface is

$$\left[\left[\frac{p}{\sigma}\right]\right] \sim \kappa. \tag{3.2}$$

There are lower order viscous terms. This yields a family of solutions $\tilde{p}=p/c$, $\tilde{\rho}=\rho/c$, and $\tilde{\sigma}=\sigma/c$. In the numerical simulations, we fix the $\dot{\gamma}=1$, $a=0.125$ and $\mu=1$, while the near-critical inertia ρ and interfacial tension σ vary by the same factors; hence in the asymptotic regime, $\mathrm{Ca.Re}\sim\rho/\sigma = \tilde{\rho}/\tilde{\sigma}$, and the problem is identical for each near-critical Re.

Figure 7 shows the temporal evolution of the dimensionless half-length L/a and angle of tilt θ. Close to Stokes flow, the drop simply elongates to steady state, and retractions when they occur are mild. For the larger Reynolds numbers, there is an initial lengthening followed by a marked retraction, with a final length which is much shorter than at low Reynolds numbers, and the angle of tilt is higher.

At larger Reynolds numbers, the drop initially wobbles, most noticeably across the narrower girth. In the transition to steady state, the drop can appear to neck, then relax back, then repeat, with the oscillations decaying. Assuming that close to the critical state drop evolution can be described by a one-dimensional model (in analogy with recent findings[13] under Stokes flow conditions), this motion is reminiscent of the mass-spring system described by

$$mx''(t) + cx'(t) + \sigma x(t) = 0, \tag{3.3}$$

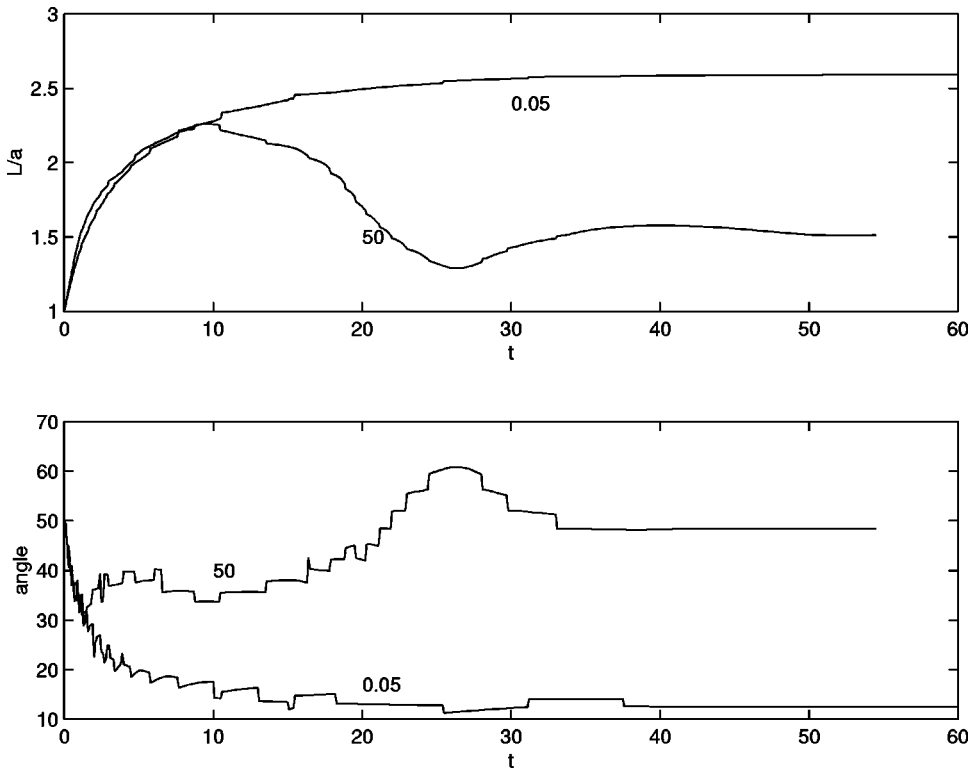

FIG. 7. Evolution of the half-length L/a and angle of tilt θ to steady state for Re=0.05, Ca=0.39, and Re=50, Ca=0.06.

where $x(t)$ denotes displacement from equilibrium (e.g., the girth B/a), m represents inertia, c is the viscous friction, and σ is the interfacial tension or restoring force. Stokes flow corresponds to an overdamped system. A large Reynolds number corresponds to an underdamped system where the solution oscillates more intensely. For an order-of-magnitude estimate, we set $m=\rho(4/3)\pi a^3$ for the mass of the drop, and use $c=6\pi\mu a$ for the Stokes drag on a sphere. In our simulations, we have used the shear rate $\dot{\gamma}=1$, so that Eq. (3.3) apart from factors translates to $\mathrm{Re.Ca}.x''(t)+\mathrm{Ca}.x'(t)+x(t)\sim 0$. This yields a period of oscillations proportional to $(\mathrm{Re.Ca})^{1/2}$.

Figure 8 shows the evolution of the half-breadth B/a. The curves for situations close to critical along the

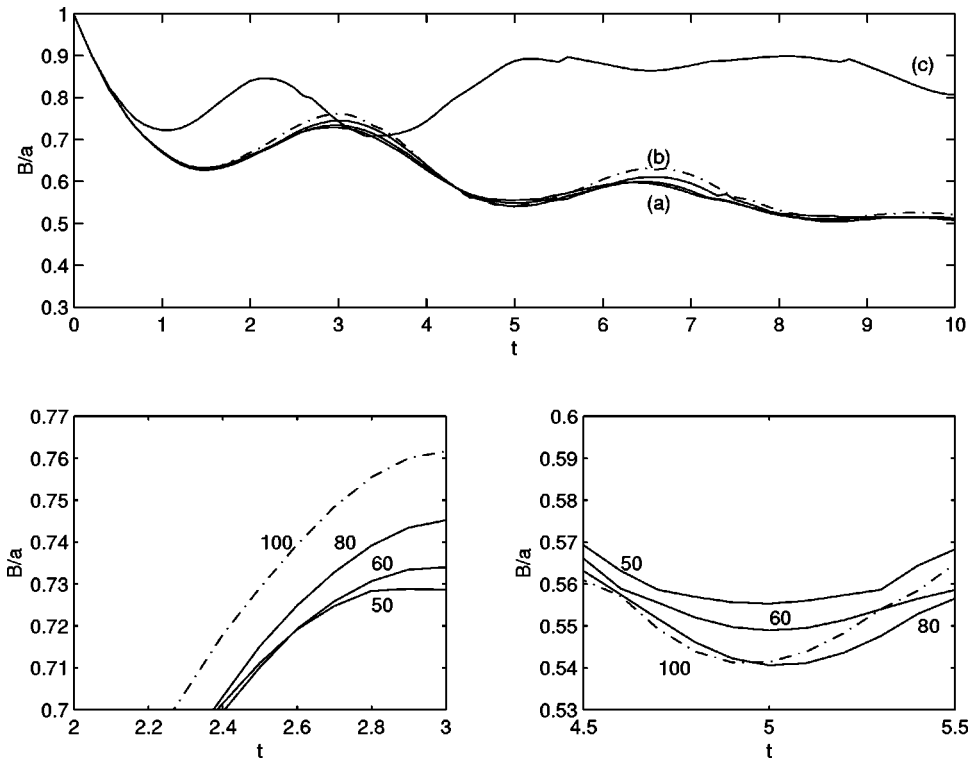

FIG. 8. Evolution of the half-breadth B/a, showing the initial oscillations before B/a climbs to equilibrium in the presence of inertia. (a) Re=50, Ca=0.061; Re=60, Ca=0.053; and Re=80, Ca=0.041 lie close together. (b) (-.-.) Re=100, Ca=0.032. (c) Re=50, Ca=0.03. The lower figures are magnifications of the first maxima and the second minima with respective values of Re.

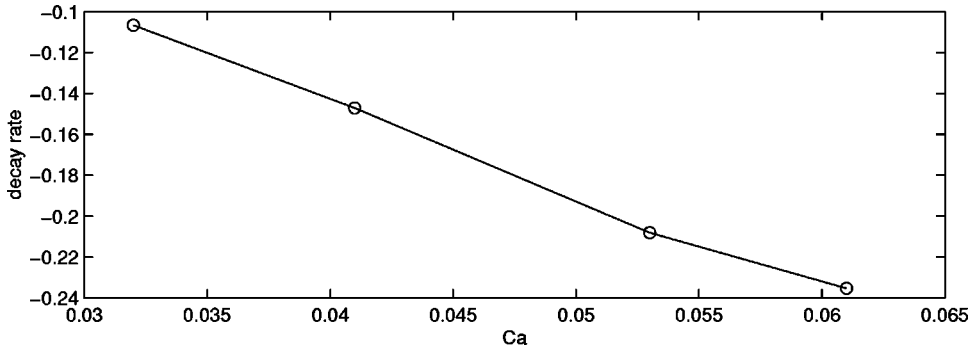

FIG. 9. Decay rate vs Ca for the evolution of the half-breadth B/a in Fig. 8 for Re=50, Ca=0.061; Re=60, Ca=0.053; Re=80, Ca=0.041; and Re=100, Ca=0.032.

asymptotic line in Fig. 1 lie close together between (a) for Re=50 and (b) for Re=100, because they approach the inviscid limit discussed for Eq. (3.1). The curve (c) is placed as an example of a situation with half the capillary number compared with the critical value. The figure shows that the period of oscillation is the same for the near-critical curves for which Re.Ca is constant. Moreover, the difference in the period for the near-critical curves and (c) at Ca=0.03 can be explained by the proportionality to $\sqrt{\text{Re.Ca}}$, by noting that the restoring force changes by a factor 2, and, therefore, we predict that the Re=50, Ca=0.061 curve would have the longer period by factor $\sqrt{2}$.

Our mass-spring model predicts solutions to have a decay rate proportional to $-1/\text{Re}$. For the asymptotic large-Re regime, this decay rate is proportional to Ca. We verify this by determining the decay rate from the first two maxima and minima in Fig. 8. Let x_0 denote the difference in height between the first maximum and first minimum, and let x_1 denote the difference between the second maximum and second minimum. The difference in t between the two maxima is Δt, a value similar to the separation of the minima. The decay rate is then proportional to $-\ln(x_0/x_1)/\Delta t$. These are plotted in Fig. 9 against the capillary number, and indeed lie on a line.

At Re=60, Fig. 10 shows a sequence of cross-sectional velocity fields at times just before the waist squeezes and distends. In (a), the drop is close to its initial stage. One vortex develops as the drop begins its initial lengthening, and the waist begins to squeeze. The velocities clearly point inwards at the waist just before B/a hits its first minimum. Figure 10(b) shows the velocities pointing outwards at the waist, during the process of expansion. Two vortices have developed, one at each end of the drop where the shear is greatest. There is also one large vortical swirl enveloping these. The drop undergoes lift at the right end, and counterlift at the left. Figure 10(c) shows the velocities pointing inwards at the waist just before B/a reaches the second squeeze. The oscillations which follow are less intense, as evident in Fig. 8. The evolution thereafter proceeds along a climb in L/a as shown in Fig. 7. When L/a begins its downhill journey, the drop surges its angle to tilt toward the vertical.

Three issues will be discussed next with respect to the numerical accuracy: the effect of spatial periodicity, distance to the walls, and spatial and temporal refinements. Spatial periodicity in the x and y directions were chosen to be $8a$ and $4a$, respectively. At Re=60, Ca=0.05 (critical Ca ≈ 0.053), the computational box in the y direction, transverse to the shear flow, was doubled and found to yield negligible differences for $L/a, B/a, \theta$ and velocity vector plots. Second, the computational box in the x direction was lengthened to examine interactions with neighboring drops. It was

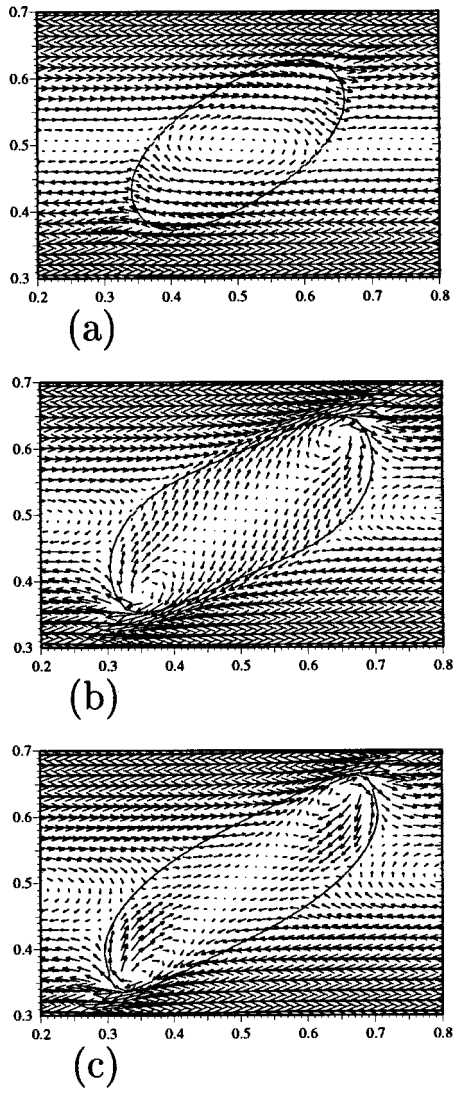

FIG. 10. Cross-sectional velocity vector fields in x-z plane, at $t=$ (a) 1, initial lengthening and before the first squeeze in B/a; (b) 2.5, before the first maximum in B/a; and (c) 4, before the second squeeze. Re=60, Ca=0.053 just below criticality.

found that increasing the x period could lead to breakup (for example, at Re=22, Ca=0.1, the $1\times0.5\times1$ domain yields steady state while $1.5\times0.5\times1$ breaks up), while for closer packing and because of the relative placement of the neighboring drops, drop elongation is evidently hindered and drops are more stable against breakup. However, the prediction for the critical point in Stokes flow is 0.42, which is close to the value reported in the literature, indicating that we have chosen a sufficiently large spatial periodicity. The influence of plate separation (discussed in detail in Ref. 7) is to induce breakup as the walls close in. For the computational box of Sec. II, Re=60, Ca=0.05 does not breakup for $d=8a,16a$. This suggests that the error due to finite wall distance should be of a few percent. The timestep size was halved and checked at Re=60, Ca=0.053, just below critical in Fig. 1, to yield stable drops. As for spatial refinement, our numerical simulations use cell sizes $\Delta x=\Delta y=\Delta z=0.125a$. Refinement can lower the critical Reynolds number slightly: for instance, at Re=60, the $96\times64\times96$ and $64\times32\times64$ cases are critical at Ca$\approx$0.049 and 0.054, respectively.

IV. CONCLUSION

Full numerical simulations were conducted with our in-house code SURFER++, based on the volume-of-fluid continuous-surface-force formulation. The critical capillary number for breakup in shear flow in the presence of inertia was found to depend on Reynolds number obeying a power law with exponent -1. Drop evolution towards steady state is initially well described by a one-dimensional mass-spring model. Near critical conditions, the steady drop configuration is in an inviscid limit, and is independent of the microphysical parameters Re and Ca near critical conditions. The process of breakup was examined in detail. It was found that the drop initially oscillates, with the period of oscillation and decay rate governed by a balance of Reynolds stress, Stokes drag and interfacial tension. The drop then lengthens and tilts up, due to what is analogous to aerodynamic lift and counterlift. The drop necks and develops the familiar dumbbells at the ends, which are tilted at a much higher angle than in Stokes flow. Thereafter, the drop experiences higher shear, which pulls apart the ends.

ACKNOWLEDGMENTS

This research was sponsored by NSF-CTS 9612308, NSF-INT 9815106, the Illinois NCSA under Grant Nos. CTS990010N, CTS990059N, and CTS990063N, and utilized the NCSA SGI Origin 2000. We are grateful to the Interdisciplinary Center for Applied Mathematics for the use of their Origin 2000. We thank Michael Renardy for discussions, Stephane Zaleski for the use of SURFER, and Jie Li for help with SURFER++. Acknowledgment is made to the donors of The Petroleum Research Fund, administered by the ACS, for partial support of this research.

[1] H. P. Grace, ''Dispersion phenomena in high viscosity immiscible fluid systems and application of static mixers as dispersion devices in such systems,'' Chem. Eng. Commun. **14**, 225 (1982).
[2] J. M. Rallison, ''The deformation of small viscous drops and bubbles in shear flows,'' Annu. Rev. Fluid Mech. **16**, 45 (1984).
[3] H. A. Stone, ''Dynamics of drop deformation and breakup in viscous fluids,'' Annu. Rev. Fluid Mech. **26**, 65 (1994).
[4] S. Kwak and C. Pozrikidis, ''Adaptive triangulation of evolving closed, or open surfaces by the advancing-front method,'' J. Comput. Phys. **14**, 61 (1998).
[5] V. Cristini, J. Blawzdziewicz, and M. Loewenberg, ''Drop breakup in three-dimensional viscous flows,'' Phys. Fluids **10**, 1781 (1998).
[6] S. Guido and M. Villone, ''Three-dimensional shape of a drop under simple shear flow,'' J. Rheol. **42**, 395 (1998).
[7] J. Li, Y. Renardy, and M. Renardy, ''Numerical simulation of breakup of a viscous drop in simple shear flow with a volume-of-fluid method,'' Phys. Fluids **12**, 269 (2000).
[8] J. U. Brackbill, D. B. Kothe, and C. Zemach, ''A continuum method for modeling surface tension,'' J. Comput. Phys. **100**, 335 (1992).
[9] B. Lafaurie, C. Nardone, R. Scardovelli, S. Zaleski, and G. Zanetti, ''Modelling merging and fragmentation in multiphase flows with SURFER,'' J. Comput. Phys. **113**, 134 (1994).
[10] J. Li, ''Calcul d'Interface Affine par Morceaux (Piecewise Linear Interface Calculation),'' C. R. Acad. Sci., Ser. IIb: Mec., Phys., Chim., Astron. **320**, 391 (1995).
[11] R. Scardovelli and S. Zaleski, ''Direct numerical simulation of free surface and interfacial flow,'' Annu. Rev. Fluid Mech. **31**, 567 (1999).
[12] T. Y. Hou, J. S. Lowengrub, and M. J. Shelley, ''The long-time motion of vortex sheets with surface tension,'' Phys. Fluids **9**, 1933 (1997).
[13] J. Blawzdziewicz, V. Cristini, and M. Loewenberg, ''Critical behavior of drop breakup in linear flows,'' Phys. Fluids (submitted).